**Article:**
Gadelovits, S.Y., Zhong, Q., Kadirkamanathan, V. et al. (2019) Uncertainty and Disturbance Estimator-Based Controller Equipped With a Time-Delayed Filter to Improve the Voltage Quality of Inverters. IEEE Transactions on Industrial Electronics, 66 (1). pp. 459-469. ISSN: 0278-0046

https://doi.org/10.1109/TIE.2018.2831182

# UDE-Based Controller Equipped with a Time-Delayed Filter to Improve the Voltage Quality of Inverters

S. Gadelovits, *Student Member, IEEE*, Qing-Chang Zhong, *Fellow, IEEE*,
V. Kadirkamanathan, and Alon Kuperman, *Senior Member, IEEE*

***Abstract*—In this paper, a two-degrees-of-freedom control structure is proposed to minimize both total harmonic distortion and tracking error of inverter output voltage, adopting a resonant tracking controller and a modified uncertainty and disturbance estimator (UDE). Owing to the two-degree-of-freedom feature of the proposed control strategy, tracking and disturbance rejection tasks are decoupled and treated almost independently. A time-delay action is introduced into a commonly adopted low-pass UDE filter to minimize the output impedance magnitude around the odd harmonics, which is typical to nonlinear loads. Once the disturbance is properly rejected, a tracking resonant controller is designed to force the output of the nominal system to follow a sinusoidal reference with near-zero amplitude and phase error. The performance of the proposed control structure is fully verified by experimental results.**

***Index Terms*—Uncertainty and disturbance estimator (UDE), inverter, resonant control, voltage quality, total harmonic distortion (THD), two degrees of freedom control.**

## I. INTRODUCTION

DC-AC converters (or inverters) have recently become a crucial element in power conversion associated applications [1]. Consequently, a vast amount of research is being conducted in the field of inverters control. Among others, reducing the total harmonic distortion (THD) and minimizing the output voltage tracking error of inverter feeding a nonlinear load are common control tasks. A variety of control strategies have been proposed in the literature to cope with the THD improvement problem [2] – [12]. It was recently understood, that THD minimization task is directly related to inverter output impedance [1]. In [13], the output impedance of an inverter was shown to be influenced by the control strategy adopted. Therefore, reducing the output impedance magnitude may enhance output voltage quality [1], [14] – [16]. It should be emphasized that when driving nonlinear loads, only the values of inverter output impedance magnitude at harmonic frequencies are of interest for THD reduction. Moreover, in single-phase inverters, odd harmonics only should be treated. In [17] – [23], multi-resonant controllers were proposed to reduce the output voltage THD by minimizing output impedance magnitude at multiples of the base operating frequency. However, classical multi-resonant control structures are of the single-degrees-of-freedom type and hence do not allow decoupling of tracking and disturbance rejection.

Disturbance observer (DOB) based controllers [24] – [26] are probably the most widely used two-degrees-of-freedom structure, allowing the aforementioned decoupling to be attained. There, the DOB nominalizes the system [27] by estimating and compensating the total uncertainty and disturbance while a tracking controller is only concerned with forcing the nominal system to follow the reference precisely. In [28], a subset of DOB named Uncertainty and Disturbance Estimator (UDE) was utilized to solve the problem of inverter output voltage quality. UDE was initially proposed in [30], elaborated in [31] – [38] and applied to a variety of control tasks [39] – [48]. Its functionality is based on the assumption that appropriate filtering can approximate any continuous uncertainty and disturbance and then compensate it by opposite phase injection. It was shown in [28] that the two-degrees-of-freedom controller may directly impose disturbance rejection through the output impedance by appropriate filter design without sensing the output current. In addition, the proposed multi-band-stop-filter structure was capable of both reducing the value of output impedance magnitude around the regions of interest and provided robustness to fundamental frequency variations. The main drawbacks of the method proposed in [28] is the effort required to obtain the required filter type and order, in addition to cumbersome structure, whose complexity increases according to the amount of harmonics to be treated (similar to multi-resonant controllers).

In this paper, a UDE-based controller equipped with a different filter is proposed to tackle the disturbance rejection task. The proposed filter resembles a classical UDE filter with a slight modification based on introducing a time delay into the estimator structure [49]. This results in a repetitive-like action [50], translated into enhanced disturbance rejection capabilities at base frequency multiples, as desired. The proposed filter is easy to implement and the resulting structure is of low complexity. In order to cope with the tracking task, a resonant controller (rather than proportional one in [28]) is utilized, allowing the transient response to be shaped according to prescribed behavior [51]. A combination of resonant and repetitive control was used in [52] – [54] using different control structures, yielding excellent performance and providing additional motivation to this work. Performance comparison between the system in [28] and the one proposed here reveals the superiority of the latter in terms of both output voltage THD and settling time under the same operating conditions. On the other hand, the robustness to base frequency variations of the former is superior to that of the algorithm proposed here.

The rest of the paper is organized as follows. The proposed control algorithm is presented in general form in Section II, while its application to enhancing voltage quality of inverters is described in Section III. Experimental validation of the proposed method is given in Section IV and conclusions are drawn in Section V.

## II. The Proposed Algorithm

Consider a stable uncertain linear SISO system with disturbance,

$$\begin{aligned}\dot{y}(t) &= -ay(t) + b\big(u(t) + f(t)\big) \\ &= -(a_n + \Delta a)\, y(t) + (b_n + \Delta b)\big(u(t) + f(t)\big),\end{aligned} \tag{1}$$

where $y(t)$ is the system output, $a_n$ and $\Delta a$ are nominal (or known) and unknown parts of $a > 0$, respectively, $u(t)$ is the control input, $b_n$ and $\Delta b$ are nominal (or known) and unknown parts of $b$, respectively, and $f(t)$ is the external disturbance. The system output $y(t)$ is desired to track a reference signal given by

$$y^*(t) = A\sin\omega_0 t \tag{2}$$

while rejecting the disturbance described by

$$f(t) = \sum_{n=1}^{\infty} F_n \sin(n\omega_0 t + \phi_n). \tag{3}$$

Rearranging (1), there is

$$\dot{y}(t) = -a_n y(t) + b_n\big(u(t) + d(t)\big) \tag{4}$$

with

$$d(t) = b_n^{-1}\big(-\Delta a y(t) + \Delta b u(t) + b f(t)\big) \tag{5}$$

denoting the total uncertainty and disturbance (TUD). Note that according to (2), (3) and (5), TUD may be expressed as

$$d(t) = \sum_{n=1}^{\infty} D_n \sin(n\omega_0 t + \theta_n). \tag{6}$$

In order to accomplish both above mentioned goals, it is proposed to utilize a two-degree-of-freedom structure by splitting the control signal as

$$u(t) = u_t(t) + u_d(t), \tag{7}$$

where $u_t(t)$ and $u_d(t)$ denote the outputs of tracking controller and disturbance observer, respectively. It is shown next that both controllers may be designed independently as long as the total available control bandwidth is not violated.

### A. Disturbance observer

Substituting (7) into (4), there is

$$\dot{y}(t) = -a_n y(t) + b_n\big(u_t(t) + u_d(t) + d(t)\big) \tag{8}$$

If $u_d(t) \approx -d(t)$, then the TUD would be cancelled and the system would become nominalized. However, $d(t)$ contains uncertain and non-measurable terms, hence it should be properly estimated. Note that TUD may be derived from (8) as

$$d(t) = b_n^{-1}\big(\dot{y}(t) + a_n y(t)\big) - u_t(t) - u_d(t). \tag{9}$$

Unfortunately, (9) cannot be utilized because of causality issues. UDE-based control estimates the TUD by passing it through a linear filter $G_f(s)$, possessing near-unity gain and near-zero phase over the frequency range where the energy of $d(t)$ is non-zero, i.e.

$$u_d(t) = d(t) * g_f(t), \tag{10}$$

where '*' is the convolution operator and $g_f(t)$ is the impulse response of $G_f(s)$. Combining (8) – (10) and rearranging gives

$$\begin{aligned}u_d(t) &= L^{-1}\left\{\frac{G_f(s)}{H_f(s)}\Big(-P_n^{-1}(s)Y(s) + U_t(s)\Big)\right\} \\ &= L^{-1}\left\{L_f(s)\Big(-P_n^{-1}(s)Y(s) + U_t(s)\Big)\right\}\end{aligned} \tag{11}$$

with $L^{-1}\{\cdot\}$ symbolizing the inverse Laplace transform operator, $Y(s)$ and $U_t(s)$ denoting Laplace transforms of $y(t)$ and $u_t(t)$, respectively, $L_f(s) = G_f(s)/H_f(s)$ signifying disturbance rejection loop gain and

$$H_f(s) = 1 - G_f(s), \quad P_n(s) = \frac{b_n}{s + a_n}. \tag{12}$$

Further substituting (11) into (8) results in

$$\dot{y}(t) = -a_n y(t) + b_n\Big(u_t(t) + L^{-1}\big\{D(s)\cdot H_f(s)\big\}\Big), \tag{13}$$

with $D(s)$ denoting the Laplace transform of $d(t)$. According to (13), in the case of $G_f(s) = 1$ (or $H_f(s) = 0$) at multiples of the base frequency $\omega_0$, the TUD will be rejected completely (cf. (3)).

In order to design suitable $G_f(s)$, note first that the following holds in steady state,

$$d(t) = d(t - T_0) \tag{14}$$

with $T_0 = 2\pi/\omega_0$, i.e.

$$u_d(t) = d(t - T_0) \tag{15a}$$

Or

$$U_d(s) = \underbrace{D(s)\cdot e^{-T_0 s}}_{G_f(s)} \tag{15b}$$

may be utilized as an estimate of TUD, i.e.

$$H_f(s) = 1 - e^{-T_0 s}, \tag{16}$$

which is a time-delayed filter extensively investigated in [55-57].

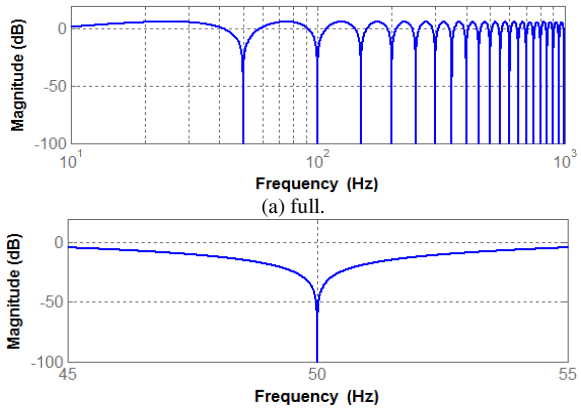


(a) full.

(b) zoomed around $1/T_0$.

Fig. 1. Bode diagram of $|H_f(s)|$ in (16) for $T_0 = 20$ ms.

Bode diagram of (16) is shown in Fig. 1 for $T_0 = 20$ ms. It is evident that $H_f(s)$ possesses zero magnitude at 50 Hz multiples, as desired. Unfortunately, the filter is characterized by infinite bandwidth as well and therefore cannot be realized as is. It is possible to restrict the filter bandwidth by modifying (15) as

$$u_d(t) = d(t - T_0) * w(t) \tag{17a}$$

or

$$U_d(s) = D(s)\cdot \underbrace{e^{-T_0 s}W(s)}_{G_f(s)} \tag{17b}$$

with $w(t)$ and $W(s)$ denoting impulse response of a low-pass filter and its corresponding Laplace transform. This gives

$$H_f(s) = 1 - e^{-T_0 s}W(s). \tag{18}$$

However, $G_f(s) \neq 1$ for any practical $W(s)$ at multiples of $\omega_0$.

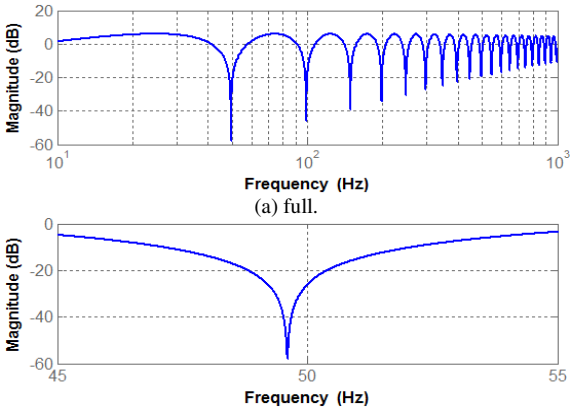


(a) full.

(b) zoomed around $1/T_0$.

Fig. 2. Bode diagram of $|H_f(s)|$ in (18) for $T_0 = 20$ ms and $W(s) = \frac{2000\pi}{s+2000\pi}$.

As a result, the magnitude of $H_f(s)$ would be different than zero at these frequencies. A Bode diagram of (18) is shown in Fig. 2(a) for $T_0 = 20$ ms and $W(s) = \frac{2000\pi}{s+2000\pi}$., As shown in Fig. 2(b), the valleys of $|H_f(s)|$ are now shifted to the left from desired positions, their corresponding values are nonzero and they are increasing for higher frequencies. While the latter may be acceptable in practical systems since $D_n$ in (6) decreases as $n$ increases, non-accurate valley positions may significantly deteriorate the disturbance rejection performance. The valley position shift is caused by the filter-induced phase lag. Therefore, it is suggested to reduce the delay time in (17) as

$$u_d(t) = d\left(t - (T_0 - \Delta T)\right) * w(t) \tag{19a}$$

or

$$U_d(s) = D(s)\cdot \underbrace{e^{-(T_0-\Delta T)s}W(s)}_{G_f(s)}, \tag{19b}$$

where $\Delta T$ is the delay of $W(s)$ at $\omega_0$. This gives

$$H_f(s) = 1 - e^{-(T_0-\Delta T)s}W(s). \tag{20}$$

A Bode diagram of (20) is shown in Fig. 3(a) for $T_0 = 20$ ms, $W(s) = \frac{2000\pi}{s+2000\pi}$ and $\Delta T = -\frac{1}{\omega_0} tg^{-1}(\frac{\omega_0}{2000\pi})$. It is evident from Fig. 3(b) that the position of the valleys of $|H_f(s)|$ are restored to the desired locations.

In case the TUD in (6) possesses odd symmetry, it would contain odd harmonics only [58]. Then, (14) may be rewritten as

$$d(t) = -d(t - \frac{T_0}{2}) \tag{21}$$

and (19) becomes

$$u_d(t) = -d\left(t - (\frac{T_0}{2} - \Delta T)\right) * w(t) \tag{22a}$$

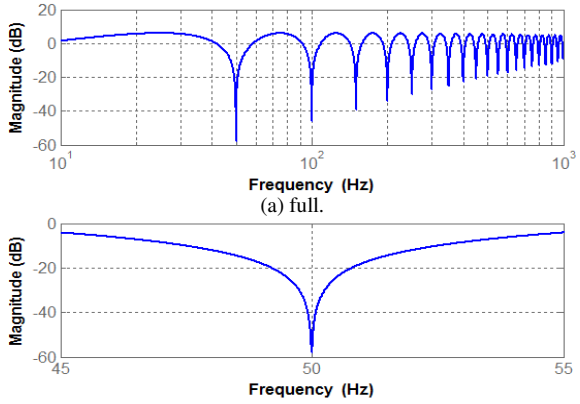


(a) full.

(b) zoomed around $1/T_0$.

Fig. 3. Bode diagram of $|H_f(s)|$ in (20) for $T_0 = 20$ ms, $W(s) = \frac{2000\pi}{s+2000\pi}$ and $\Delta T = -\frac{1}{\omega_0} tg^{-1}(\frac{\omega_0}{2000\pi})$.

or

$$U_d(s) = D(s)\cdot \underbrace{(-e^{-(\frac{T_0}{2}-\Delta T)s}W(s))}_{G_f(s)}. \tag{22b}$$

This gives

$$H_f(s) = 1 + e^{-(\frac{T_0}{2}-\Delta T)s}W(s). \tag{23}$$

Bode diagram of (23) is shown in Fig. 4(a) for $T_0 = 20$ ms, $W(s) = \frac{2000\pi}{s+2000\pi}$ and $\Delta T = \frac{1}{2000\pi}$. The valleys of $|H_f(s)|$ are located at odd multiples of $\omega_0$, as shown in Fig. 4(b). The values of $|H_f(s)|$ valleys are similar to these of (20), however for the case of digital implementation the amount of memory used to implement the delay in (23) is half of that needed for implementing (20).

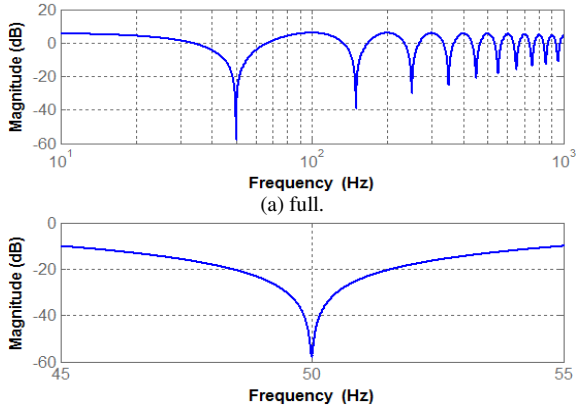


(a) full.

(b) zoomed around $1/T_0$.

Fig. 4. Bode diagram of $|H_f(s)|$ in (23) for $T_0 = 20$ ms, $W(s) = \frac{2000\pi}{s+2000\pi}$ and $\Delta T = -\frac{1}{\omega_0} tg^{-1}(\frac{\omega_0}{2000\pi})$.

TABLE I
VALUES OF $\Delta T$ FOR BUTTERWORTH FILTERS OF DIFFERENT ORDERS

| Order | $G_f(s)$ | $\Delta T$ |
|---|---|---|
| 1 | $\frac{\omega_F}{s+\omega_F}$ | $-\frac{1}{\omega_0} tg^{-1}(\frac{\omega_0}{\omega_F})$ |
| 2 | $\frac{\omega_F^2}{s^2+\sqrt{2}\omega_F\cdot s+\omega_F^2}$ | $-\frac{1}{\omega_0} tg^{-1}\left(\frac{\sqrt{2}\omega_0\omega_F}{\omega_F^2-\omega_0^2}\right)$ |
| 3 | $\frac{\omega_F^3}{s^3+2\omega_F s^2+2\omega_F^2 s+\omega_F^3}$ | $-\frac{1}{\omega_0} tg^{-1}(\frac{2\omega_F^2\omega_0-\omega_0^3}{\omega_F^3-2\omega_0^2\omega_F})$ |

It is interesting to explore the influence of increasing filter order on disturbance rejection loop gain. Table I summarizes Butterworth filter $G_f(s)$ of orders 1 – 3 and corresponding values of $\Delta T$. Bode diagrams of $H_f(s)$ for $T_0$ = 20 ms and $\omega_F$ = 2000π rad/s are shown in Fig. 5(a) for the three filters in Table I along with zooms around the first (Fig. 5(b) and third (Fig. 5(c)) base frequency multiples.

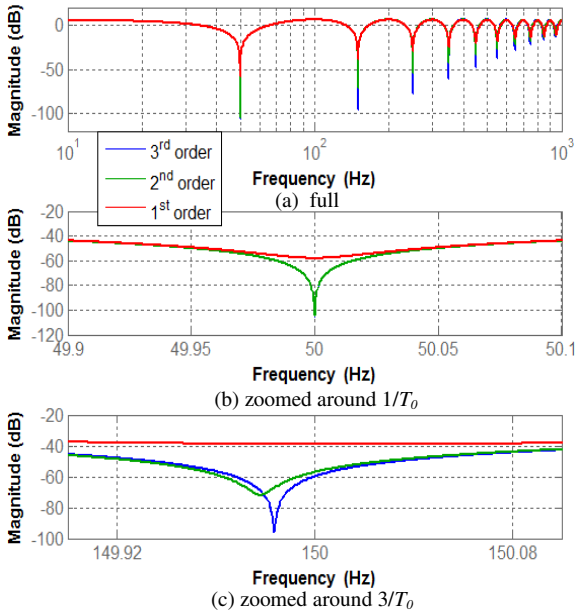


Fig. 5. Bode diagram of $|H_f(s)|$ in (23) for $T_0$ = 20 ms and different $W(s)$ and $\Delta T$ from Table I.

The following may be observed:
- Increasing the filter order above 1 greatly improves the disturbance rejection at relevant frequencies.
- The values of $|H_f(\omega_0)|$ are quite similar for UDE utilizing second and third order filters.
- Higher order filter utilization leads to better disturbance rejection at higher base frequency multiples.
- Location of resonant peaks is shifted for $n \geq 3$. This is due to the fact that the phase shift correction via $\Delta T$ is performed according to $n$ = 1. Therefore, in case rejection of $n^{\text{th}}$ harmonic is the most significant, $\Delta T$ should be calculated accordingly.

### B. Tracking controller

If the system is properly nominalized by the disturbance rejection controller, then $u_d(t) \approx -d(t)$ and

$$\dot{y}(t) \approx -a_n y(t) + b_n u_t(t). \tag{21}$$

In order to make sure that $y(t)$ follows the reference (2), the desired response is formulated as

$$y(t) = \left(1 - e^{-\omega_t t}\right) y^*(t) = A\left(1 - e^{-\omega_t t}\right)\sin \omega_0 t, \tag{22}$$

with $\omega_t$ denoting the magnitude convergence rate. Hence,

$$T_y(s) = \frac{Y(s)}{Y^*(s)} = \frac{2\omega_t s + \omega_t^2}{(s+\omega_t)^2 + \omega_0^2} \tag{23}$$

is the desired complementary sensitivity function with $Y^*(s)$ symbolizing the Laplace transform of $y^*(t)$, indicating that transient response influences the envelope only without affecting either frequency or phase. On the other hand, if the output of the tracking controller $C_t(s)$ is given by

$$u_t(t) = L^{-1}\left\{C_t(s)\left(Y^*(s) - Y(s)\right)\right\}, \tag{24}$$

then

$$T_y(s) = \frac{C_t(s)P_n(s)}{1 + C_t(s)P_n(s)} = \frac{L_t(s)}{1 + L_t(s)} \tag{25}$$

with $P_n(s)$ defined in (12) and $L_t(s)$ symbolizes tracking loop gain, derived from (23) as

$$L_t(s) = \frac{2\omega_t s + \omega_t^2}{s^2 + \omega_0^2}. \tag{26}$$

An interested reader is referred to [51] for detailed analysis of (26). Combining (23) with (25) taking into account (12) yields tracking controller transfer function,

$$C_t(s) = P_n^{-1}(s)L_t(s) = \frac{(s + a_n)\left(2\omega_t s + \omega_t^2\right)}{b_n\left(s^2 + \omega_0^2\right)}. \tag{27}$$

Note that the obtained controller is characterized by infinite gain at $\omega_0$ as expected, yet is derived intuitively rather than following the generalized integrator theory. The overall control action $u(t)$ is then described by (7) with (11) and (24). Rearranging, it may be expressed in a two-degrees of freedom form as

$$u(t) = y^*(t) * L^{-1}\{H_{FF}(s)\} - y(t) * L^{-1}\{H_{FB}(s)\} \tag{28}$$

with

$$H_{FF}(s) = \frac{C_t(s)}{1 - G_f(s)}, \quad H_{FB}(s) = \frac{C_t(s) + G_f(s)P_n^{-1}(s)}{1 - G_f(s)}. \tag{29}$$

The total nominal loop gain of the system is then given by

$$L_{tot}(s) = P_n(s)H_{FB}(s) = \frac{L_t(s)}{1 - G_f(s)} + L_f(s). \tag{30}$$

For the boundary case of $G_f(s)$ = 0 (no disturbance rejection loop), $L_{tot}(s) = L_t(s)$. On the other hand, in case $\omega_t$ = 0 (no tracking loop), $L_{tot}(s) = L_f(s)$. Hence, for a given desired phase margin (or control bandwidth), trade-off between disturbance rejection (set by the bandwidth of $L_f(s)$) and tracking (set by the bandwidth of $L_t(s)$) is expected and must be taken into account when designing the controller.

## III. Application to Improving the Voltage Quality of Inverters

Consider a single-phase LC filter based inverter, powered from a dc source $v_{DC}$. The inverter feeds a nonlinear load, drawing current given in general form by

$$i_O(t) = \sum_{\substack{n=1 \\ n\,odd}}^{\infty} I_n \sin(n\omega_0 t + \varphi_n) \tag{31}$$

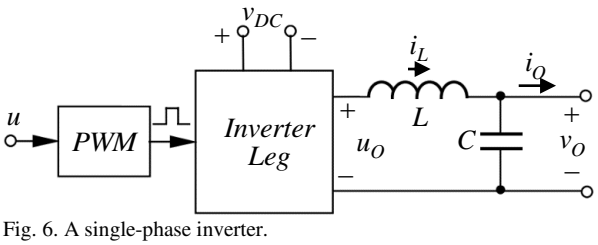


Fig. 6. A single-phase inverter.

The control signal $u$ is converted into a PWM signal, driving the converter leg as shown in Fig. 6. The inverter leg output voltage, inductor current and capacitor voltage are denoted as $u_0$, $i_L$ and $v_O$, respectively. The control goal is forcing the inverter output voltage

$$v_O(t) = \sum_{\substack{n=1 \\ n\,odd}}^{\infty} V_n \sin(n\omega_0 t + \psi_n), \tag{32}$$

to track the reference given by

$$v_O^*(t) = V_M \sin \omega_0 t \tag{33}$$

by operating with unity displacement factor (achieved by the tracking controller) while minimizing the total harmonic distortion (ensured by disturbance observer), defined by

$$THD_V = V_1^{-1}\sqrt{\sum_{\substack{n=3 \\ n\,odd}}^{\infty} V_n^2} = V_1^{-1}\sqrt{\sum_{\substack{n=3 \\ n\,odd}}^{\infty} \left(I_n |Z_{On}|\right)^2}, \tag{34}$$

where $|Z_{On}| = |Z_O(jn\omega_0)| = |V_n/I_n|_{VM=0}$ denotes the value of inverter output impedance magnitude at $n$-th multiple of base frequency. Obviously, it is desired to have $|Z_{On}| \to 0$ in order to achieve good disturbance rejection at relevant frequencies. In order to cope with the task, it is proposed to utilize a cascaded dual-loop control structure (similarly to [28]), utilizing a PI controller as an inner (inductor current) loop compensator (P controller was utilized in [28]) and a two-degrees-of-freedom controller, revealed in the preceding Section, as the outer (capacitor voltage) loop regulator. Table II summarizes the numerical values of system parameters, used in the simulations and experiments presented later.

TABLE II
NOMINAL SYSTEM PARAMETER VALUES

| Parameter | Value | Units |
|---|---|---|
| Switching frequency, $T_S^{-1}$ | 15 | *kHz* |
| Filter inductance, $L$ | 3.4 | *mH* |
| Filter capacitance, $C_n$ | 30 | *μF* |
| Base frequency, $\omega_0$ | 100π | *rad/s* |
| DC link voltage, $v_{DC}$ | 195 | *V* |
| Reference magnitude, $V_M$ | 110√2 | *V* |

### A. *Inner loop controller design and analysis*

Inductor current dynamics are given by

$$L\frac{di_L(t)}{dt} = u(t-T_d)v_{DC}(t) - v_O(t) \tag{35}$$

with $T_d$ denoting the overall sampling and switching delay. Defining an auxiliary control input $u'(t)$ so that

$$u(t) = \frac{1}{v_{DC}(t)}\left(u'(t) + v_O(t)\right), \tag{36}$$

while assuming that $T_d^{-1}$ is much higher than bandwidth of $v_{DC}$, the current plant is linearized as

$$L\frac{di_L(t)}{dt} \approx u'(t-T_d) + \underbrace{v_O(t-T_d) - v_O(t)}_{\Delta v_O}. \tag{37}$$

In order to attenuate the remaining disturbance $\Delta v_O$, proportional-integrative controller

$$C_I(s) = K_{PI}\left(\frac{1+\tau_I s}{s}\right) \tag{38}$$

is utilized, i.e. $u'(t) = L^{-1}\left\{C_I(s)\left(i_L^*(s) - i_L(s)\right)\right\}$. Current loop gain and complementary sensitivity function are then obtained as

$$LG_I(s) = \frac{K_{PI}\left(1+\tau_I s\right)}{Ls^2}e^{-T_d s} \tag{39}$$

and

$$T_I(s) = \frac{I_L(s)}{I_L^*(s)} = \frac{K_{PI}L^{-1}\left(1+\tau_I s\right)}{s^2 e^{T_d s} + K_{PI}L^{-1}\tau_I s + K_{PI}L^{-1}}, \tag{40}$$

respectively, with $I_L^*(s)$ denoting inductor current reference signal, generated by the outer loop controller.

The design of $C_I(s)$ is then carried out following [59]. Adopting double-update PWM and sampling as close as possible to the PWM update instance, total transport and computation delay of $T_d = 45\mu s$ may be achieved [28], leading to $K_{PI} = 7.94\cdot10^4$ and $\tau = 6.53\cdot10^{-4}$. This gives current loop bandwidth of 2450Hz with 45° phase margin and 7dB gain margin, as shown in Fig. 7. Complementary sensitivity function actually acts as voltage loop actuator and must be taken into account during outer loop compensator design.

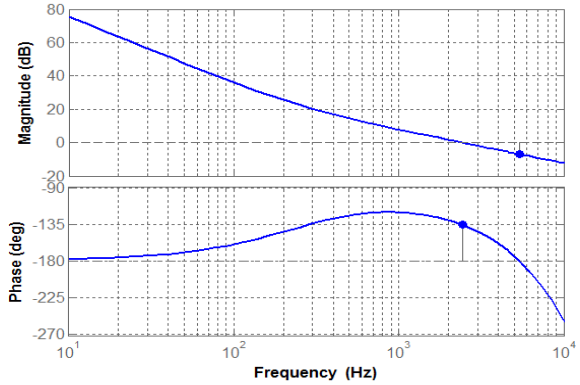


Fig. 7. Current loop gain Bode diagram.

### B. *Voltage controller design and analysis*

Output voltage dynamics are given by

$$\frac{dv_O(t)}{dt} = \underbrace{(C_n^{-1} + \Delta C)}_{C}\left(i_L(t) - i_O(t)\right), \tag{41}$$

i.e. referring to (4), $a_n = 0$, $b_n = C_n^{-1}$, $y(t) = v_O(t)$, $u = i_L(t)$, $P_n(s) = (C_n s)^{-1}$ and $d(t) = C_n(Ci_O(t) - \Delta Ci_L(t))$. The two-degrees-of-freedom controller (cf. Fig. 8) design details are hence as follows.

#### *B1. Tracking controller*

The tracking controller should be designed so that the tracking loop gain crossover frequency is at least ten times higher than the resonant frequency [51], i.e.

$$\left|L_t(j10\omega_0)\right| = 1. \tag{42}$$

Substitution into (26) yields $\omega_t \approx 4.8\omega_0$. Combining (24), (27) and (42) yields the output of the tracking controller as [51]

$$u_t(t) = L^{-1}\left\{\underbrace{C_n\frac{9.6\omega_0 s^2 + 23\omega_0^2 s}{s^2+\omega_0^2}}_{C_t(s)}\left(V_O^*(s) - V_O(s)\right)\right\}. \tag{43}$$

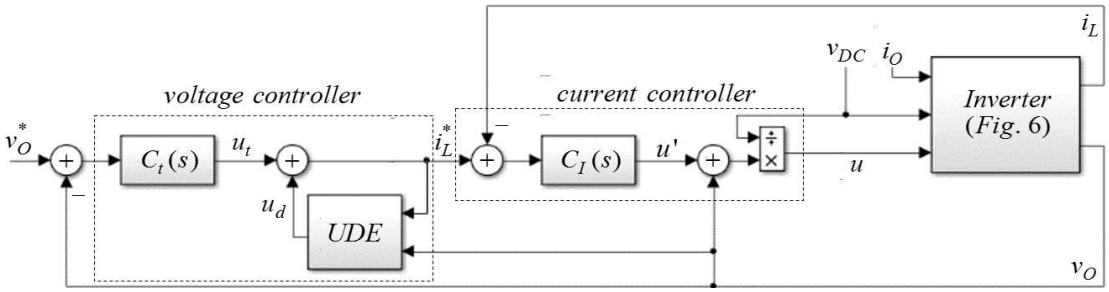


Fig. 8. Block diagram of the proposed control structure.

*B2. Disturbance observer*

According to (11), disturbance observer output is given by

$$u_d(t) = L^{-1}\left\{\frac{G_f(s)}{1-G_f(s)}\left(-C_n sV_O(s)+U_t(s)\right)\right\} \tag{44}$$

with $G_f(s)$ listed in Table I and $u_t(t)$ defined in (43). The current reference is then formed by the sum of (43) and (44) (cf. (8)) as

$$i_L^*(t) = L^{-1}\left\{-C_n\frac{sG_f(s)}{1-G_f(s)}V_O(s)+\frac{1}{1-G_f(s)}U_t(s)\right\}. \tag{45}$$

In order to determine the maximum attainable value of $\omega_F$, required for disturbance rejection filter $G_f(s)$ selection, recall that $i_L^*$ rather than $i_L$ is set by the voltage controller. Therefore, current loop complementary sensitivity function $T_I(s)$ acts as the voltage loop actuator and must be properly taken into account by modifying the total nominal loop gain of the system as

$$L_{tot}(s) = T_I(s)\left(\frac{L_t(s)}{1-G_f(s)}+L_f(s)\right). \tag{46}$$

Corresponding inverter output impedance is derived as [28]

$$\begin{aligned} Z_O(s) &= \frac{1-G_f(s)}{sC\left(1+G_f(s)\left(T_I(s)-1\right)\right)+C_t(s)T_I(s)} \\ &\overset{T_I(s)\to 1}{=} \underbrace{\frac{1}{sC+C_t(s)}}_{Z_t(s)}\left(1-G_f(s)\right) = Z_t(s)H_f(s), \end{aligned} \tag{47}$$

formed by two terms: $Z_t(s)$, related to the plant and tracking controller and $H_f(s)$, related to UDE filter.

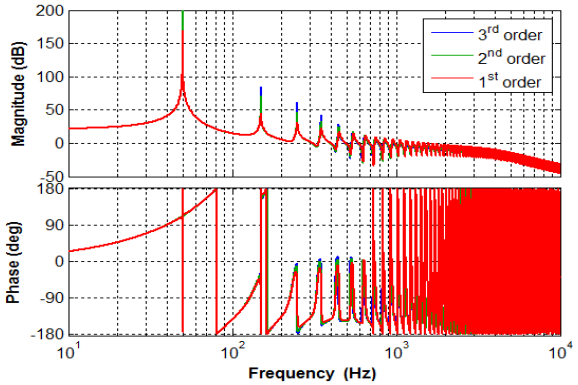


Fig. 9. Bode diagram of $L_{tot}(s)$ in (46) for the filters in Table I with cutoff frequencies in Table III.

Since significant parameter variations are not expected in the voltage plant, phase margin (PM) of 30° and gain margin (GM) of 5dB are chosen as minimum values for stability assurance. If larger margins are required the system may be redesigned at the expense of slight reduction of $\omega_t$ or $\omega_F$. Resulting values of $\omega_F$ along with the resulting stability margins are summarized in Table III. Bode diagram of corresponding overall loop gain $L_{tot}(s)$ is given in Fig. 9. It is well-evident that rising the filter order increases the loop gain magnitude (i.e. improves the system disturbance rejection capability) at odd multiples of $\omega_0$. The output impedance $Z_O(s)$ and its forming terms (cf. (47)) are shown in Fig. 10 for the 3rd order filter. As expected, $H_f(s)$ possesses resistive behavior at odd multiples of $\omega_0$ while $Z_O(s)$ is capacitive at $\omega_0$ and slightly inductive at odd multiples of $\omega_0$ due to influence of $Z_t(s)$.

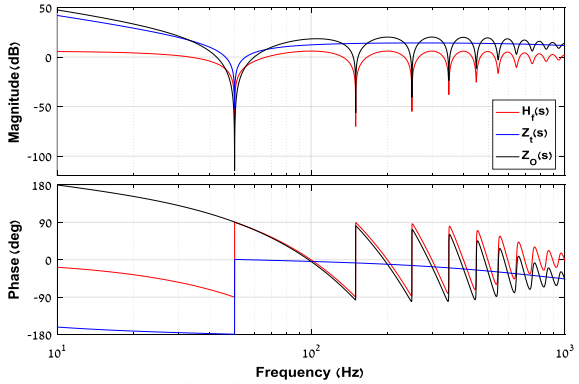


Fig. 10. Bode diagram of $|Z_O(s)|$ in (47) for the filters in Table I with cutoff frequencies in Table III.

TABLE III
CUT-OFF FREQUENCIES AND STABILITY MARGINS FOR BUTTERWORTH FILTERS OF DIFFERENT ORDERS

| Order | $\omega_F$, rad/s | *PM*, ° | *GM, dB* |
|---|---|---|---|
| 1 | $2\pi \cdot 690$ | 30 | 5 |
| 2 | $2\pi \cdot 670$ | 30 | 10.4 |
| 3 | $2\pi \cdot 640$ | 30 | 12.6 |

## IV. VERIFICATION

In order to confirm the revealed control structure, modified Texas Instruments High Voltage Single Phase Inverter Development Kit (TIDK) was employed. Inverter parameters are similar to the values given in Table II. The control system was implemented digitally using a Concerto F28M35 control card. Experimental setup is shown in Fig. 11.

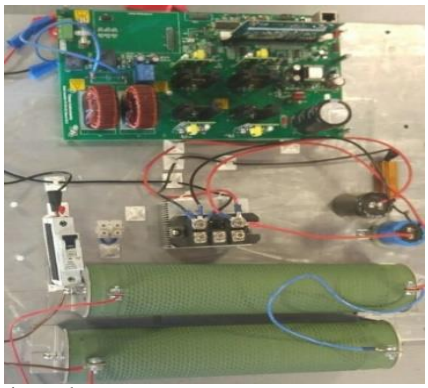

Fig. 11. Experimental setup.

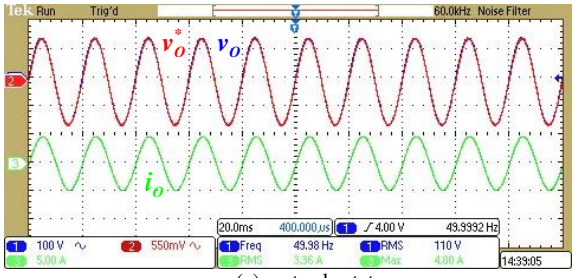


(a) steady state.

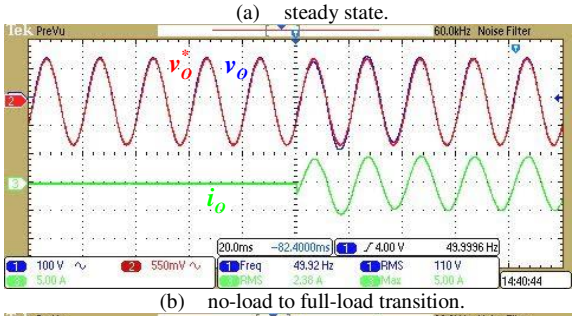


(b) no-load to full-load transition.

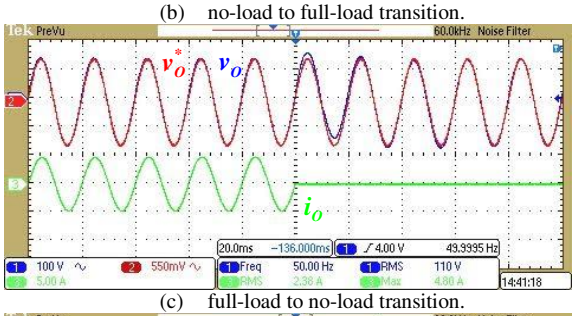


(c) full-load to no-load transition.

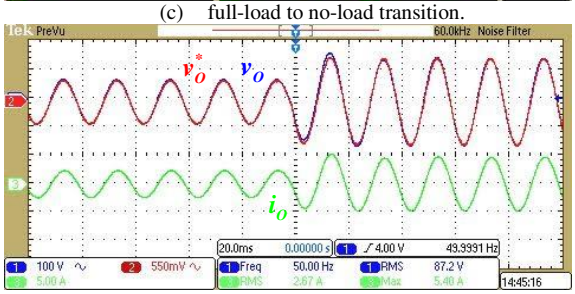


(d) reference magnitude variation under load.

Fig. 12. Experimental results: Operation under linear load.

### A. *Operation with linear load*

In order to examine the operation with linear load, the inverter was terminated by a 33Ω resistor. A third order Butterworth filter based UDE was employed. Fig. 12 presents the results of steady state operation (Fig. 12(a)) as well as full load to no load (Fig. 12(b)) and no load to full load (Fig. 12(c)) transitions. In addition, Fig. 12(d) demonstrates the system response to reference magnitude variation from 50% to 100% of nominal value. It may be concluded that the system performs well in both steady state and transient regimes. Output voltage THD under linear load was found to be 0.87%.

### B. *Operation with nonlinear load*

In order to inspect the operation under nonlinear load, the 33Ω resistor was replaced by a diode rectifier, driving a 50Ω, 940µF parallel RC load (250W) with a crest factor of 3.2~3.5, depending on the inverter internal impedance. For testing transients, the load resistor has been replaced with 100Ω resistor to limit the inrush current. Performance utilizing, first, second and third order Butterworth filter based UDEs were examined. Fig. 13 presents the time domain results of steady state operation while Fig. 14 compares respective experimental frequency domain distributions and total harmonic distortions of the output voltage for all three cases. As predicted, $THD_V$ reduces with the increase of filter order, which mainly affects the 3rd and 5th harmonics.

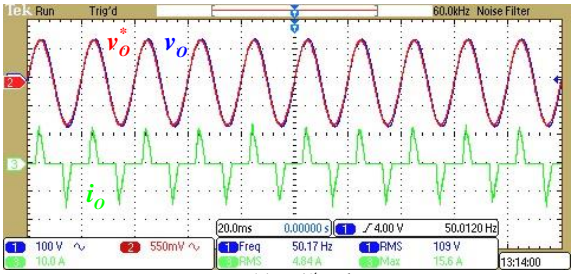


(a) 1st order.

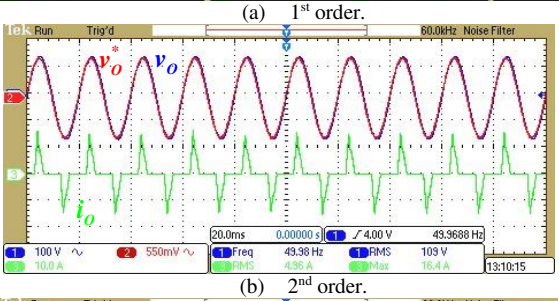


(b) 2nd order.

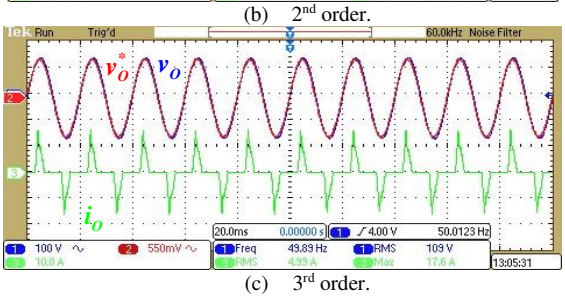


(c) 3rd order.

Fig. 13. Experimental results: Steady-state operation under nonlinear load for different orders of $G_f(s)$.

Fig. 15 presents the full load to no load and no load to full load transitions for the third order Butterworth filter based UDE. The no load to full load transient is usually the worst one to expect. The settling time here is formed by a half-cycle-delay, used in the UDE, filter response time and load transient. According to the results, the performance may be

considered satisfactory when the impressive steady state performance is taken into account.

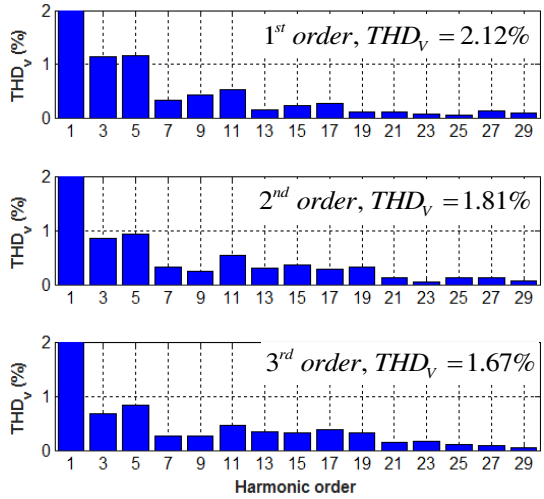


Fig. 14. Experimental results: Output voltage spectra comparison for different orders of $G_f(s)$.

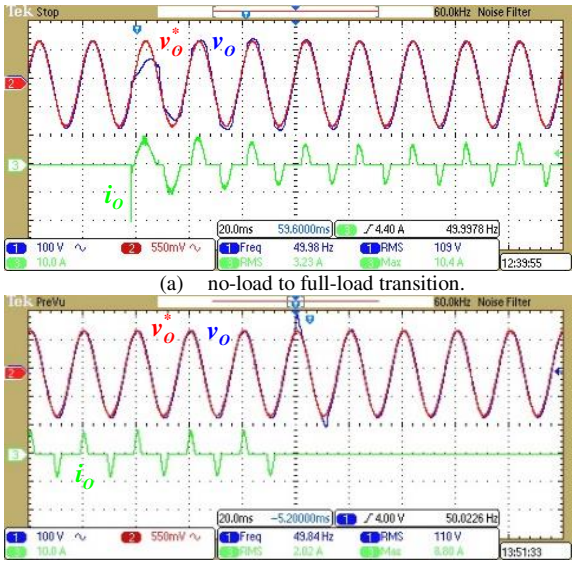


(a) no-load to full-load transition.

(b) full-load to no-load transition.

Fig. 15. Experimental results: Transient performance under nonlinear load for 3rd order Butterworth filter based UDE.

Steady-state system operation under nonlinear load system was also verified under fundamental frequency deviation up to ±1Hz to examine the robustness. Experimental results are shown in Fig. 16 with corresponding values of $THD_V$ indicated. $THD_V$ is noticeably affected by base frequency variations.

### C. Comparison with multi-band-stop filter based UDE

As mentioned above, in a recent paper [28] a similar dual-loop control structure was proposed, utilizing a proportional controller as a current loop regulator and a different two-degree of freedom regulator as a voltage controller. A proportional nominal voltage loop tracking controller was employed, while a UDE equipped with a multi-band-stop filter was utilized for disturbance rejection. The hardware setup and other operational parameters (switching frequency and load) were similar to the ones in this paper.

Performance comparison results of control structure in [28] and the one proposed in the paper (utilizing a 3rd order Butterworth filter) is summarized in Fig. 17. Frequency domain distributions and total harmonic distortions of the output voltage are compared in Fig. 17(a) for nominal base frequency operation. It may be concluded that the control structure proposed in this paper outperforms the one in [28] in terms of $THD_V$. However, if the base frequency were to vary, the algorithm in [28] becomes superior to the one proposed here, as shown in Fig. 17(b). This is because the control structure in [28] was designed especially for ensuring robustness to base frequency variations. The algorithm proposed in this paper outperforms the one in [28] in terms of transient response speed as well, as shown in Fig. 17(c),

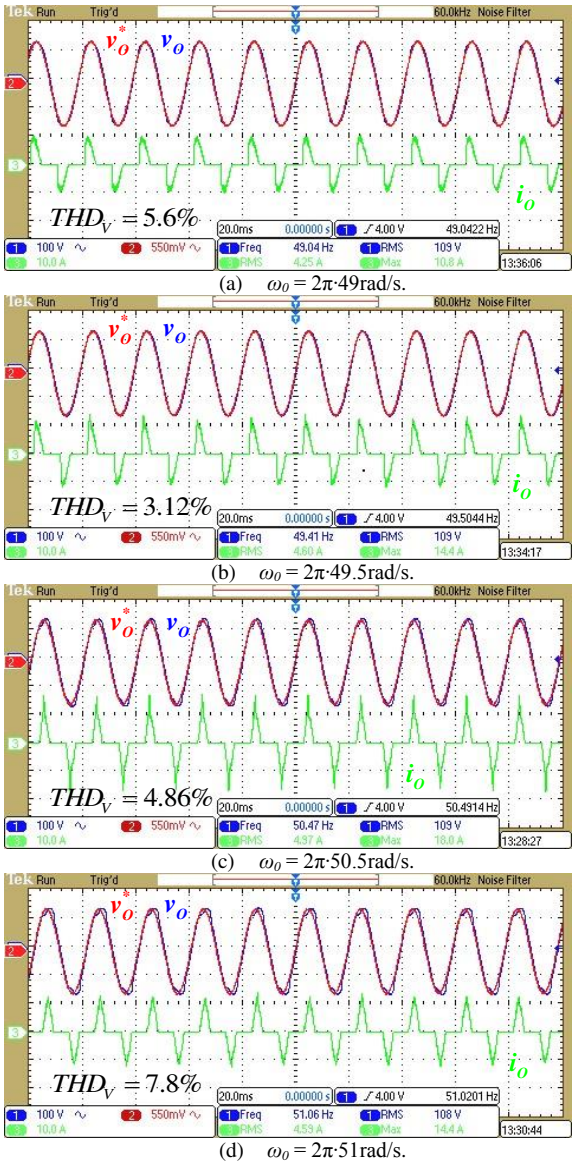


(a) $\omega_0 = 2\pi \cdot 49$rad/s.

(b) $\omega_0 = 2\pi \cdot 49.5$rad/s.

(c) $\omega_0 = 2\pi \cdot 50.5$rad/s.

(d) $\omega_0 = 2\pi \cdot 51$rad/s.

Fig. 16. Experimental results. Steady state operation under ±1Hz base frequency deviation.

which presents the output voltage tracking errors for no load to full load to no load transients.

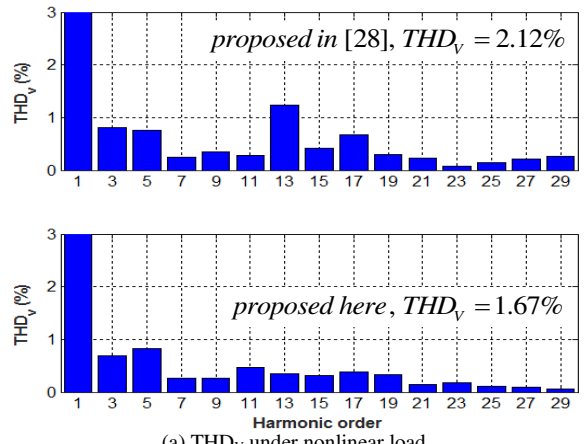


(a) $THD_V$ under nonlinear load.

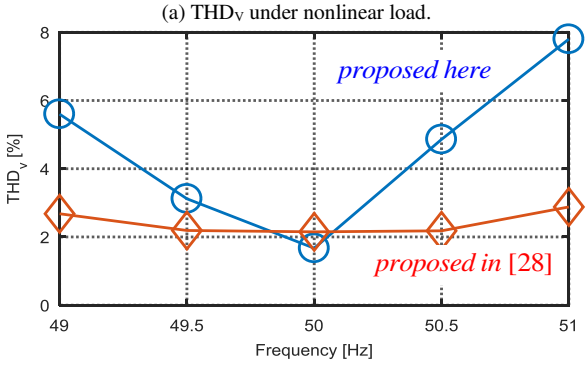


(b) Robustness to frequency variations.

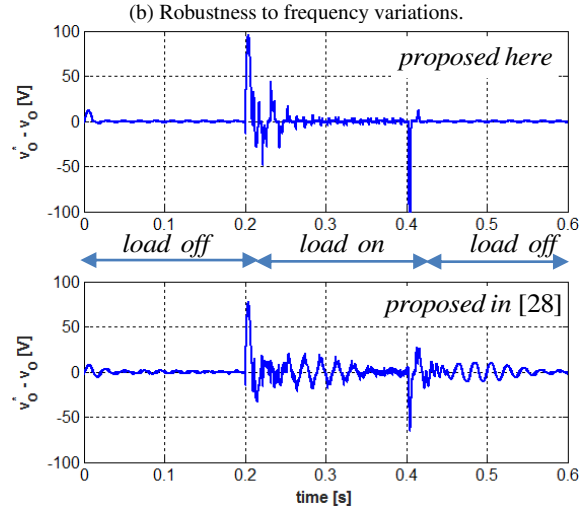


(c) Tracking error.

Fig. 17. Results of comparison with the method proposed in [28].

## V. Conclusions

In this paper, a two-degrees-of-freedom control structure was proposed for enhancing the output voltage quality of inverters, allowing tracking and disturbance rejection problems to be decoupled. A modified Uncertainty and Disturbance Estimator, based on time-delay filter, was utilized to tackle the disturbance rejection task. Employing the proposed filter has led to minimization of inverter output impedance magnitude around the harmonics of interest, leading to enhanced disturbance rejection capabilities. Once the total uncertainty and disturbance was accurately estimated and eliminated by the proposed disturbance observer, it was possible to impose desired tracking performance by a suitable resonant tracking controller, designed according to prescribed nominal transient behavior. Theoretical findings were fully supported by experimental results. Possibility to improve robustness to base frequency variations using multiple delay filters [55] - [57], [60] will be examined in future work.

## Acknowledgement

Shlomo Y Gadelovits was supported by the Doctoral Prize Scholarship of the Department of Automatic Control and Systems Engineering, The University of Sheffield.

## References

[1] Q.-C. Zhong and T. Hornik, *Control of Power Inverters in Renewable Energy and Smart Grid Integration*. New York, NY, USA: Wiley-IEEE Press, 2013.

[2] O. Kukrer, H. Komurcugil and A. Doganalp, "A three-level hysteresis function approach to the sliding-mode control of single-phase UPS inverters," *IEEE Trans. Ind. Electron.*, vol. 56, no. 9, pp. 3477-3486, Sep. 2009.

[3] H. Komurcugil, "Rotating-sliding-line-based sliding-mode control for single-phase UPS inverters," *IEEE Trans. Ind. Electron.*, vol. 59, no. 10, pp. 3719-3726, Oct. 2012.

[4] A. Kawamura, R. Chuarayapratip and T. Haneyoshi, "Deadbeat control of PWM inverter with modified pulse patterns for UPS," *IEEE Trans. Ind. Electron.*, vol. 35, no. 2, pp. 295-300, May 1988.

[5] H. Komurcugil, N. Altin, S. Ozdemir and I. Sefa, "Lyapunov-function and proportional-resonant-based control strategy for single-phase grid-connected VSI with LCL filter," *IEEE Trans. Ind. Electron.*, vol. 63, no. 5, pp. 2838-2849, May 2016.

[6] L. Padmavathi and P. A. Janakiraman, "Self-tuned feed-forward compensation for harmonic reduction in single-phase low-voltage inverters," *IEEE Trans. Ind. Electron.*, vol. 58, no. 10, pp. 4753-4762, Oct. 2011.

[7] H. Komurcugil, N. Altin, S. Ozdemir and I. Sefa, "An extended Lyapunov-function-based control strategy for single-phase UPS inverters," *IEEE Trans. Power Electron.*, vol. 30, no. 7, pp. 3976-3983, Jul. 2015.

[8] B. Zhang, D. Wang, K. Zhou, and Y. Wang, "Linear phase lead compensation repetitive control of a CVCF PWM inverter," *IEEE Trans. Ind. Electron*., vol. 55, no. 4, pp. 1595–1602, Apr. 2008.

[9] A. Kavousi, B. Vahidi, R. Salehi, M. Bakhshizadeh, N. Farokhnia, and S. Fathi, "Application of the bee algorithm for selective harmonic elimination strategy in multilevel inverters," *IEEE Trans. Power Electron*., vol. 27, no. 4, pp. 1689–1696, Apr. 2012.

[10] Q.-C. Zhong, "Harmonic droop controller to reduce the voltage harmonics of inverters," *IEEE Trans. Ind. Electron.*, vol. 60, no. 3, pp. 936-945, Mar. 2013.

[11] J. Lim, C. Park, J. Han and Y. Lee, "Robust tracking control of a three-phase DC-AC inverter for UPS applications," *IEEE Trans. Ind. Electron.*, vol. 61, no. 8, pp. 4142 – 4151, Aug. 2014.

[12] P. Cortes, G. Ortiz, J. Yuz, J. Rodriguez, S. Vasquez and L. Franquelo, "Model predictive control of an inverter with output LC filter for UPS applications," *IEEE Trans. Ind. Electron*., vol. 56, no. 6, pp. 1875 – 1883, Jun. 2009.

[13] J. M. Guerrero, L. G. de Vicuna, J. Matas, M. Castilla, and J. Miret, "Output impedance design of parallel-connected UPS inverters with wireless load-sharing control," *IEEE Trans. Ind. Electron*., vol. 52, no. 4, pp. 1126–1135, May. 2005

[14] J. M. Guerrero, J. Matas, L. G. de Vicuna, M. Castilla, and J. Miret, "Decentralized control for parallel operation of distributed generation inverters using resistive output impedance," *IEEE Trans. Ind. Electron*., vol. 54, no. 2, pp. 994–1004, Nov. 2007.

[15] H. Deng, R. Oruganti and D. Srinivasan, "A simple control method for high-performance UPS inverters through output impedance reduction," *IEEE Trans. Ind. Electron*., vol. 55, no. 2, pp. 888 – 898, Feb. 2008.

[16] Q.-C. Zhong and Y. Zeng, "Control of inverters via a virtual capacitor to achieve capacitive output impedance," *IEEE Trans. Power Electron.*, vol. 29, no. 10, pp. 5568-5578, Oct. 2014.

[17] C. Zhang, J. Guerrero, J. Vasquez and C. Seniger, "Modular plug'n'play control architectures for three phase inverters in UPS applications," *IEEE Trans. Ind. Appl*., vol. 52, no. 3, pp. 2405 – 2414, May 2016.

[18] D. De and V. Ramanarayanan, "A proportional+multiresonant controller for three phase four wire high frequency link inverter," *IEEE Trrans. Power Electron*., vol. 25, no. 4, pp. 899 - 906, Apr. 2010.

[19] V.-T. Phas and H.-H. Lee, "Control strategy for harmonic elimination in stand-alone DFIG applications with nonlinear loads," *IEEE Trans. Power Electron*., vol. 26, no. 9, pp. 2662 - 2675, Sep. 2011.

[20] R. Cardenas, C. Juri, R. Pena, P. Wheeler and J. Clare, "The application of resonant controllers to four-leg matrix converters feeding unbalanced or nonlinear loads," *IEEE Trans. Power Electron*., vol. 27, no. 3, pp. 1120 - 1128, Mar. 2012.

[21] L. F. A. Pereira, J. V. Flores, G. Bonan, D. F. Coutinho and J. M. G. da Silva Jr., "Multiple resonant controllers for UPS – a systematic robust control design approach," *IEEE Trans. Ind. Electron*., vol. 61, no. 3, pp. 1528 - 1538, Mar. 2014.

[22] A. Lidozzi, L. Solero, S. Bifaretti and F. Crescimbini, "Sinusoidal voltage shaping of inverter-equipped stand-alone generating units," *IEEE Trans. Ind. Electron*., vol. 62, no. 6, pp. 3557 - 3568, Jun. 2015.

[23] A. Lidozzi, M. Di Benedetto, S. Bifaretti, L. Solero and F. Crescimbini, "Resonant controllers with three degrees of freedom for AC power electronics converters," *IEEE Trans. Ind. Appl*., vol. 51, no. 6, pp. 4595 - 4604, Nov./Dec. 2015.

[24] W.-H. Chen, K. Ohnishi and L. Guo, "Advances in Disturbance/Uncertainty estimation and attenuation," *IEEE Trans. Ind. Electron*., vol. 62, no. 9, pp. 5758 – 5762, Sep. 2015.

[25] J. Yang, W.-H. Chen and Z. Ding, "Disturbance observers and applications," *Trans. Inst. Meas. Control*, vol. 38, no. 6, pp. 621 – 624, 2016.

[26] W.-H. Chen, J. Yang, L. Guo and S. Li, "DOB control and related methods – an overview," *IEEE Trans. Ind. Electron*., vol. 63, no. 2, pp. 1083 –1095, Feb. 2016.

[27] A. Kuperman, Y. Horen and S. Tapuchi, "Input-output nominalization of linear plants with slow varying uncertainties," *COMPEL - Int. J. Comp. Math. Electr. Electron. Eng.*, vol. 29, no. 1, pp. 72-89, 2010.

[28] S. Gadelovits, Q.-C. Zhong V. Kadirkamanathan and A. Kuperman, "UDE-based controller equipped with a multi-band-stop filter to improve the voltage quality of inverters," *IEEE Trans. Ind. Electron*., vol. 64, no. 9, pp. 7433 – 7443, Sep. 2017.

[29] Q.-C. Zhong and D. Rees, "Control of uncertain LTI systems based on UDE," *ASME J. Dyn. Syst. Meas. Control*, vol. 126, pp. 905–910, 2004.

[30] Q.-C. Zhong, A. Kuperman, and R. K. Stobart, "Design of UDE-based controllers from their two-degree-of-freedom nature," *Int. J. Robust Nonl. Control*, vol. 21, no. 17, pp. 1994–2008, 2011.

[31] R. K. Stobart, A. Kuperman and Q.-C. Zhong, "UDE–based control for uncertain LTI-SISO systems with state delays," *ASME J. Dyn. Syst. Meas. Control*, vol. 133, pp. 024502-1-3, 2011.

[32] V. Deshpande, S. Phadke, "Control of uncertain nonlinear systems using UDE," *ASME J. Dyn. Syst. Meas. Control*, vol. 134, pp. 024501-1-7, 2012.

[33] A. Kuperman and Q.-C. Zhong, "Robust control of uncertain nonlinear systems with state delays based on UDE," *Int. J. Robust Nonl. Control*, vol. 21, no. 1, pp. 79–92, Mar. 2010.

[34] T.S. Chandar and S. Talole, "Improving the performance of UDE-based controller using a new filter design," *Nonl. Dyn.*, vol. 77, no. 3, pp. 753 – 768, 2014.

[35] A. Kuperman, "Design of α-filter based UDE controllers considering finite control bandwidth," *Nonl. Dyn.*, vol. 81, no. 1, pp. 411 – 416, 2015.

[36] A. Kuperman, "Comments on 'Design of α-Filter based UDE controllers considering finite control bandwidth'," *Nonl. Dyn.*, vol. 85, pp. 693 – 698, 2016.

[37] B. Ren, Q.-C. Zhong and J. Dai, "Asymptotic reference tracking and disturbance rejection of UDE-based robust control," *IEEE Trans. Ind. Electron*., vol. 64, no. 4, pp. 3166 – 3176, Apr. 2017.

[38] A. Kuperman and Q.-C. Zhong, "UDE-based linear robust control for a class of nonlinear systems with application to wing rock motion stabilization," *Nonl. Dyn.*, vol. 81, no. 1, pp. 789 – 799, 2015.

[39] R. Sanz, P. Garcia, Q.-C. Zong and P. Albertos, "Predictor-based control of a class of time-delay systems and its application to quadrotors,"*IEEE Trans. Ind. Electron.*, DOI 10.1109/TIE.2016.2609378.

[40] J. Chen, B. Ren and Q.-C. Zhong, "UDE-based trajectory tracking control of piezoelectric stages," *IEEE Trans. Ind. Electron.*, vol. 63, no. 10, pp. 6450-6459, Oct. 2016.

[41] A. Kuperman, "Uncertainty and disturbance estimator-assisted control of a two-axis active magnetic bearing," *Trans. Inst. Meas. Control*, vol. 38, no. 6, pp. 764 – 772, 2016.

[42] L. Sun, Q.-C. Zhong and K. Y. Lee, Control of a class of industrial processes with time delay based on a modified uncertainty and disturbance estimator," *IEEE Trans. Ind. Electron.*, vol. 63, no. 11, pp. 7018-7028, Nov. 2016.

[43] B. Ren, Q.-C. Zhong and J. Chen, "Robust control for a class of nonaffine nonlinear systems based on the uncertainty and disturbance estimator," *IEEE Trans. Ind. Electron.*, vol. 62, no. 9, pp. 5881-5888, Sep. 2015.

[44] B. Ren, Y. Wang, and Q.-C. Zhong, "UDE-based control of variable-speed wind turbine systems," *Int. J. Control*, vol. 90, no. 1, pp. 137 – 152, 2017.

[45] I. Aharon, D. Shmilovitz and A. Kuperman, "Robust output voltage control of multimode non inverting DC-DC converter," *Int. J. Control*, vol. 90, no. 1, pp. 110–120, Jan. 2017.

[46] J. Ren, Y. Ye, G. Xu, Q. Zhao and M. Zhu, "Uncertainty and disturbance estimator-based current control scheme for PMSM drives with a simple parameter tuning algorithm," *IEEE Trans. Power Electron.*, DOI: 10.1109/TPEL.2016.2607228.

[47] Q.-C. Zhong Y.Wang and B. Ren, "UDE-based robust droop control of inverters in parallel operation," *IEEE Trans. Ind. Electron*., DOI: 10.1109/TIE.2017.2677309.

[48] I. Aharon, D. Shmilovitz and A. Kuperman, "Uncertainty and disturbance estimator based controllers design under finite control bandwidth constraint," *IEEE Trans. Ind. Electron*., vol. 65, no. 2, pp. 1439 – 1449, Feb. 2018.

[49] N. Alshek, M. Elkayam and A. Kuperman, "Estimation of harmonic disturbances with time delay UDE based controller," in Proc. *Int. Conf. Sci. Electr. Eng. (ISCEE)*, Nov. 16 – 18, Eilat, Israel, 2016.

[50] A. Lidozzi, C. Ji, L. Solero, F. Crescimbini and P. Zanchetta, "Load-adaptive zero-phase-shift direct repetitive control for stand-alone four-leg VSI," *IEEE Trans. Ind. Appl*., vol. 52, no. 6, pp. 4899-4908, Nov.-Dec. 2016.

[51] A. Kuperman, "Proportional-resonant current controllers design based on desired transient performance," *IEEE Trans. Power Electron*., vol. 30, no. 10, pp. 5341 – 5345, Oct. 2015.

[52] A. Lidozzi, C. Ji, L. Solero, P. Zanchetta and F. Crescimbini, "Resonant–repetitive combined control for stand-alone power supply units," *IEEE Trans. Ind. Appl*., vol. 51, no. 6, pp. 4653-4663, Nov.-Dec. 2015.

[53] R. Ortega, G. Garcerá, E. Figueres and O. Carranza, "Comparative analysis of two control schemes for reduction of the THD in voltage applied to a single-phase inverter with nonlinear loads," in Proc. *38th IEEE Ann. Conf. Ind. Electron. Soc*., pp. 5613-5618, Montreal, Canada, 2012.

[54] R. Ortega, O. Carranza, J. C. Sosa, V. H. García and N. Y. Ortega, "Application control configurations in a photovoltaic inverter operating in a microgrid," in Proc. *41st IEEE Ann. Conf. Ind. Electron. Soc*., pp. 1014-1019, Yokohama, Japan, 2015.

[55] Q.-C. Zhong, "Control of integral process with dead time – Part 3: Deadbeat disturbance response," *IEEE Trans. Aut. Contr*., vol. 48, no. 1, pp. 153 - 159, Jan. 2003.

[56] Q.-C. Zhong "Time Delay Control & Its Applications", Shanghai Jiao Tong University, China, 1999 [in Chinese].

[57] Q.-C. Zhong, X. Y. Jian and Q. Jia "Time delay filter-based deadbeat control of process with dead-time. "*Industrial & Engineering Chemistry Research,* 39, no. 6, pp 2024-2028, 2000.

[58] R. Grino and R. Costa-Castello, "Digital repetitive plug-in controller for odd-harmonic periodic references and disturbances," *Automatica*, vol. 41, pp. 153 – 157, 2005.

[59] D. G. Holmes, T. A. Lipo, B. P. McGrath and W. Y. Kong, "Optimized design of stationary frame three phase AC current regulators," *IEEE Trans. Power Electron*., vol. 24, no. 11, pp. 2417 – 2426, Nov. 2009.

[60] M. Steinbuch, "Repetitive control for system with uncertain period-time," *Automatica*, vol. 38, pp. 2103 – 2109, 2002.